Exogenous Protein Delivery of Ionic Liquid-Mediated HMGB1 Coating on Titanium Implants

Alexandra Arteaga,[⊥] Dineli T. S. Ranathunga,[⊥] Jiayi Qu, Claudia C. Biguetti, Steven O. Nielsen, and Danieli C. Rodrigues*

ACCESS | Metrics & More | Article Recommendations | Supporting Information

ABSTRACT: Strategies for modifying titanium (Ti) implant surfaces are becoming increasingly popular to enhance osseointegration during acute and inflammatory healing stages. In this study, two dicationic imidazolium-based ionic liquids (IonLs) containing phenylalanine and methionine anions (IonL-Phe(1,10-bis(3-methylimidazolium-1-yl)decane diphenylalanine) and IonL-Met-(1,10-bis(3-methylimidazolium-1-yl)decane dimethionine)) were investigated to stably deliver exogenous proteins on Ti to promote osseointegration. The protein selected for this study is High-Mobility Group Box 1 (HMGB1), which recruits inflammatory and mesenchymal stem cells to the implantation site, contributing to healing. To explore IonL−Ti interactions and HMGB1 stability on the IonL-coated surface, experimental characterization techniques including X-ray photoelectron spectroscopy, scanning electron microscopy, dynamic scanning calorimetry (DSC), and liquid chromatography mass spectrometry (LC−MS) were used along with molecular dynamics (MD) computer simulations to provide a detailed molecular level description. Results show well-structured IonL molecules on the Ti surface that impact protein crystallization and coating morphology. IonL cations and anions were found to bind strongly to oppositely charged residues of the protein. LC−MS/MS reveals that HMGB1 B-box lysine residues bind strongly to the IonLs. Stronger interactions of HMGB1 with Ion-Phe in contrast to IonL-Met results in greater retention capacity of HMGB1 in the IonL-Phe coating. Overall, this study provides evidence that the selected IonLs strongly interact with HMGB1, which can be a potential surface treatment for bone-implantable Ti devices.
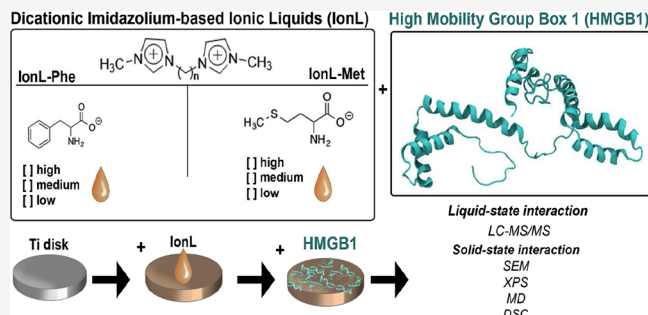
1. INTRODUCTION

Bone-implantable devices such as orthopedic and dental implants have been engineered for fixation and/or retention purposes, with a focus on osseointegration capacity, mechanical properties, and long-term biocompatibility when placed in living bone.[1] Among the different biomaterials used for the fabrication of orthopedic implants, titanium (Ti) and its alloys (i.e., Ti-6Al-4V) combine ideal bulk properties (i.e., modulus of elasticity comparable to bone and high tensile and compressive strength), surface properties, biocompatibility due to its oxide layer (TiO_2), and corrosion resistance.[2] Rutile is a thermodynamically stable form of titanium dioxide crystalline polymorph.[3] The rutile (110) surface is the most stable crystalline phase, and the implants with rutile phase exhibit better biocompatibility and osseointegration than the anatase phase implant.[3,4] The bulk of the material used for the implantable device determines its mechanical properties, while its surface characteristics, such as topography and chemical composition, guide favorable biological interactions between the implant and the host tissue.[5] It is important to note that the early biological events upon biomaterial implantation are greatly influenced by material surface properties.[6,7] This

ultimately determines early tissue response and bone formation at the bone/implant interface and, consequently, the ability of this interface to adapt to long-term continuous load interactions.[8] Despite the high corrosion resistance of Ti implants, challenging conditions in vivo (i.e., chronic inflammation and/or higher host susceptibility to infection) can initiate metal dissolution from the Ti surface, which may result in early implant failures.[9−13] Thus, research is moving toward Ti surface modifications for immunomodulation and/or osteogenesis to achieve improved early osseointegration and mitigate early failures related to deficient host responses.[14−16]

Different methods and molecules have been used for Ti surface modification in order to improve osseointegration, such as classic osteogenic factors (BMP-2 and BMP-7) incorporated into different types of carriers (e.g., sodium tri-polyphosphate,

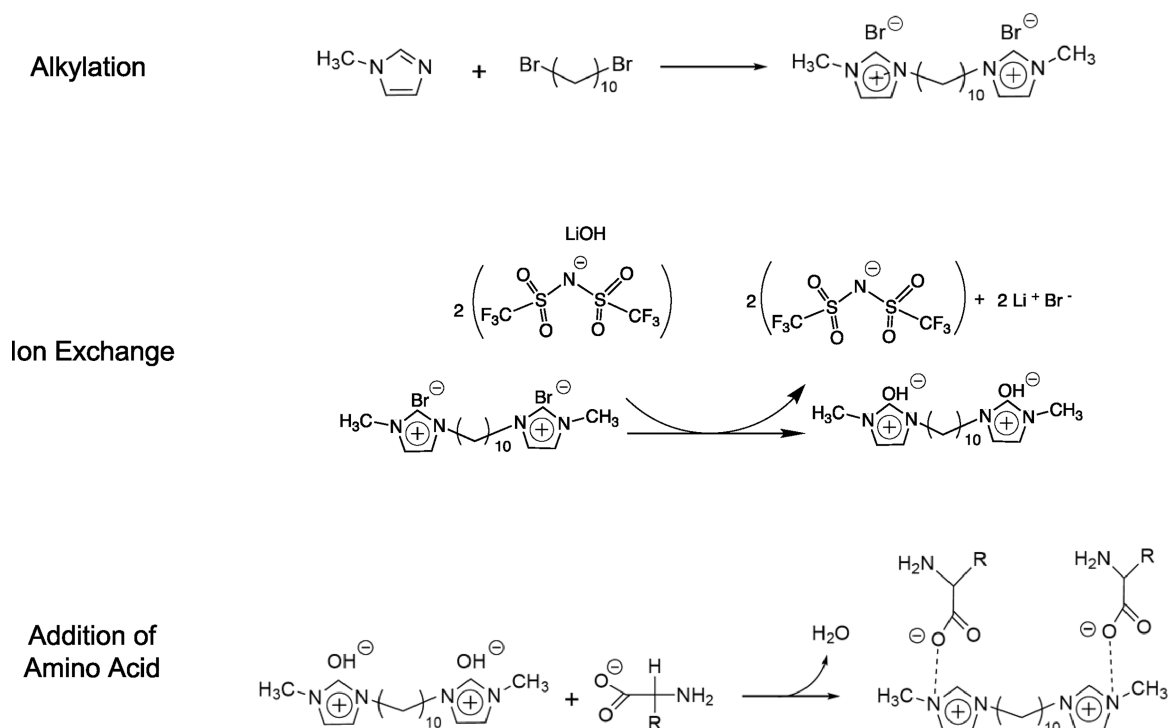**Alkylation**

Ion Exchange

Addition of Amino Acid
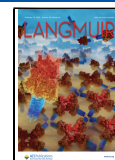
Figure 1. Chemical synthesis of ionic liquids following the Fukumoto et al.[38] and Shirota et al.[39] methods as shown in previous literature.[15]

calcium phosphate) on Ti surfaces.[17,18] Ideally, these surface modifications allow the therapeutic molecule to be delivered locally with the capacity for further specialization through spatial targeting mechanisms.[19] However, the desired bio-activity of a mediator can be affected by the vehicle/carrier used to deliver or immobilize the exogenous molecule to the peri-implant space.[20] For example, proteins tend to adsorb onto implant surfaces, which can affect the protein interaction with desired host receptors.[21] Thus, it is hypothesized that dicationic imidazolium-based ionic liquids (IonLs) may serve as a suitable local delivery system to carry immunomodulatory/regenerative soluble mediators on Ti surfaces.

IonLs are low-temperature molten salts that are being increasingly studied due to the tunability of the amphiphilic cation and anion structures, which ultimately affect the physical, chemical, and biological properties of these molecules.[22] Ionic liquid films have been investigated for use on the surface of titanium[14,23−28] and zirconia[29] as multifunctional coatings. IonL-coated surfaces demonstrated a decreased coefficient of friction (COF), lower wear volume loss and scarring, and less corrosion as well as exhibited anti-biofilm formation properties.[23,25,26] In previous studies from our lab, coating morphology and interactions between TiO$_2$ using different compositions of IonLs was demonstrated at the microscopic level, revealing strong interactions with titanium surfaces.[5] On Ti surfaces, IonLs promote anti-corrosive and tribological properties while being biocompatible to mammalian cells. Our recent in vivo studies indicated that two formulations of dicationic imidazolium-based IonLs (with phenylalanine [IonL-Phe] and methionine [IonL-Met] anions) exhibited biocompatibility upon subcutaneous implantation in Lewis rats,[14] leading to a low degree inflammatory response followed by tissue healing, making both formulations suitable for applications on Ti implantable devices as a coating. Furthermore, the in silico coating profile observed in our

previous studies[3] suggests that ionic material would provide a suitable temporal control for protein adsorption to the Ti surface. This presents a unique opportunity to improve the osseointegration of Ti-based biomaterials by utilizing IonL as a method to immobilize key immunomodulatory/osteogenic proteins.

When the implant is exposed to the living bone upon surgical placement, the implant surface will initiate a sequence of protein adsorption.[6,10,30] This protein layer includes cell adhesion and hemostasis molecules as well as damage associated molecular patterns (DAMPs), among other inflammatory mediators and growth factors.[31−33] This adsorbed protein layer also constitutes the first provisional matrix and the primary interaction site driving cell homing and activation to the biomaterial surface, which is essential in achieving successful early events of osseointegration.[30] Combining previous findings from in vitro and in vivo studies, the initial protein layer is a sophisticated system composed of many molecular components, including bone-like proteins, growth factors, immunological mediators,[34] and DAMPs such as High-Mobility Group Box 1 (HMGB1).[32] HMGB1 has been demonstrated as a key component in Ti osseointegration[32] and bone healing post-fracture.[35] Indeed, when HMGB1 is passively released by cells at the site of injury, it has been shown to play multiple roles on tissue healing and osseointegration: (1) blood clot formation,[32] (2) organization of the provisional matrix on an implant surface since it acts in synergy with thrombin to promote fibrin network formation,[32] (3) triggering of an inflammatory response through the receptor for advanced glycation end products (RAGE) and toll-like receptor 4 (TLR4),[35] and (4) formation of a heterocomplex with the chemokine CXCL12, which is critical for the mobilization of mesenchymal stem cells (MSC) to sites of healing.[36,37] Thus, it is predicted that the bioactivity and
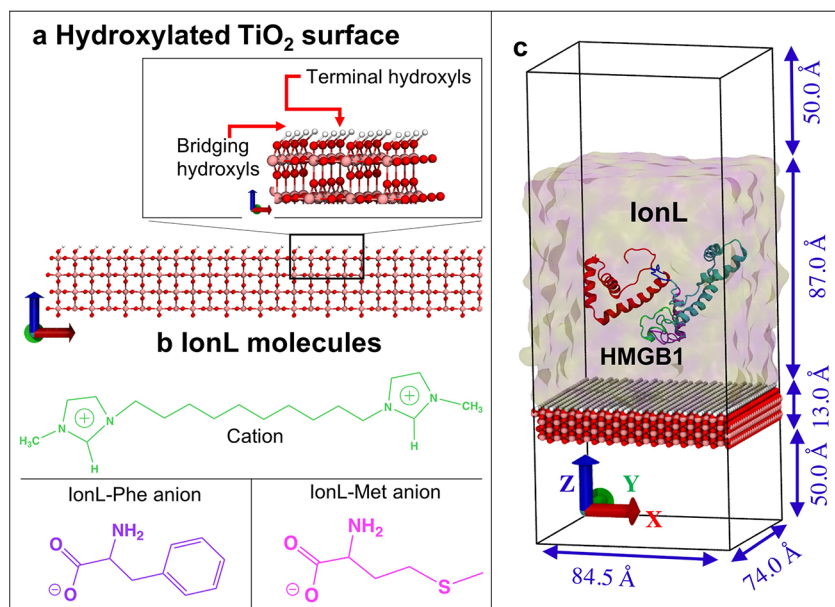
Figure 2. (a) Model of the 100% hydroxylated electrically neutral TiO$_2$ surface generated with computer simulations. Coloring is as follows: surface oxygen atoms (red), surface titanium (pink), and surface hydrogen (white). (b) Chemical structures of IonL-Phe and IonL-Met. (c) Size and initial configuration of the simulation box prepared for the molecular dynamic simulations.

clinical efficacy of biomaterial surfaces can be improved by delivering exogenous HMGB1 on bone-implantable surfaces.

Our previous results[3] have shown that in the absence of IonL films, the sequence of HMGB1 involved in MSC recruitment can permanently adhere to the oxidized surface of Ti (TiO$_2$) and be inactivated, which is an undesirable effect. Regarding coating development, it is hypothesized that IonLs with amino acid-based anions can temporarily anchor the HMGB1 onto the Ti surface. IonL films were selected due to their multifunctionality, stability,[25,27] in vitro cell compatibility,[29] and in vivo tissue interactions.[14] The goal of this study is to provide a comprehensive molecular-level understanding of how dicationic imidazolium-based ionic liquid coatings interact with exogenous HMGB1 protein to result in an effective surface treatment for bone-implantable Ti devices.

2. EXPERIMENTAL SECTION

2.1. Materials and Methods. *2.1.1. IonL Coating Preparation.* The synthetic procedure for dicationic imidazolium based-IonLs is well established in the literature.[15] The first reaction is a nucleophilic substitution reaction where there is an alkylation of methylimidazole. In the second step, the anion is exchanged through a metathesis reaction to change the halide to an inorganic anion. In this step, the cation and anion were separately dissolved from salt forms in a solvent and allowed to stir with heating to about 25 °C. The third step follows the Fukumoto et al. method, where imidazolium hydroxide was prepared using anion exchange resin followed by the addition of amino acids dissolved in water, synthesizing monocationic IonLs with amino acids as anions. Using these techniques, 1,10-bis(3-methylimidazolium-1-yl)decane diphenylalanine (IonL-Phe) and 1,10-bis(3-methylimidazolium-1-yl)decane dimethionine (IonL-Met) were synthesized and characterized using established protocols.[14,15,24,25,27,29,38,39] Both IonLs were characterized using 1H nuclear magnetic resonance spectroscopy (NMR) (Bruker Avance III-HD 600 NMR, Bruker, Billerica, MA, USA), and the data found were in accordance with the literature.[28] The chemical synthesis strategy can be seen in Figure 1, and the selected ionic liquids are shown in Figure 2b.

2.1.2. Sample Preparation. Ti disc (TiO$_2$, 5 mm ø × 2 mm, McMaster Carr, Elmhurst, IonL, USA) cross-sectional areas were rough-polished sequentially using 240, 360, 600, 800, and 1200 grit SiC paper and then fine-polished using a 1 μm polycrystalline diamond followed by 0.05 μm nanometer alumina on a polisher mounted with an automated polishing head (NANO 1000T and FEMTO 1100, Pace Technologies). Specimens were then cleaned by ultrasonication while sequentially immersed for 15 min in acetone, deionized water, and ethanol. Specimens were then dried in an oven for 24 h at 65 °C. Ti discs were dip-coated in varied concentrations of ethanolic IonL-Phe or IonL-Met solutions for 10 min to achieve three different doses denoted low, medium, and high, as shown in Table 1.

Table 1. Dip-Coating Concentrations Needed to Achieve Desired Doses of IonL on Specimens[14]

IonL	IonL concentration in coating solution (mM)	amount of IonL on discs after drying (μmol)	dose
Met	9	0.2	low
Met	50	1	medium
Met	100	2	high
Phe	50	0.1	low
Phe	165	0.5	medium
Phe	305	1	high

After 10 min, the discs were removed from solution at a constant rate of 60 μm/s with the assistance of a motorized stage (TA Instruments, New Castle, DE, USA) to achieve a homogeneous and uniform coating and then were placed in an oven at 65 °C to dry for 48 h. For the amounts of pure IonL present on discs after drying, a correlation was made, using UV–vis Spectroscopy, between coating concentrations and redissolved aliquot concentrations by using a calibration curve for both IonL-Phe and IonL-Met in ethanol at 0, 0.1, 0.25, 0.5, 1.0, 10, 25, 50, 100, and 250 mM. Final coating concentration was obtained from these data points using linear interpolation (Table 1). Subsequently, the discs were drop-coated with 2.5 μg of HMGB1 (a physiologically relevant dose[35]) diluted in 2.5 μL of deionized water and dried for 1 h at room temperature.

2.2. Molecular Dynamics Model Preparation and Simulation Details. *2.2.1. Model Preparation.* The complete HMGB1 structure consisting of 215 amino acids was modeled using the I-TASSER online web server utilizing the available tandem HMG box domain PDB (2YRQ) structure as a template.[3] A disulfide bond was

made between the C23 and C45 cysteine residues.[40] The CHARMM36 all-atom force field parameters were used to represent the protein. The surface oxygens of TiO_2 are usually hydroxylated by, among other things, moisture from the air.[24] Therefore, following the procedure in Ranathunga et al.,[3] an electrically neutral 100% hydroxylated four-layered slab of rutile (110) TiO_2 with size 84.45 Å × 74.00 Å × 12.82 Å in the x-, y-, and z-directions was built (Figure 2a). The hydroxyl groups were connected to the Ti atoms on the surface, and the bridging oxygen atoms were replaced by hydroxyl groups (Figure 2). All terminal and bridging surface hydroxyl groups were modeled using flexible bond and bend potentials, while the bulk atoms were fixed in place during the simulations. The Lennard−Jones parameters of all the hydroxyls were identical to those for the TIP3P water model. The atomic charges and the Lennard−Jones parameters of Ti and O were taken from our previous study.[3] The bond stretching and bending parameters were adopted from Brandt et al.[41] The IonL 1,10-bis(3-methylimidazolium-1-yl) decane cation parameters were obtained from Gross et al.,[42] and the phenylalanine and methionine anions were modeled using the CHARMM36 force field (Figure 2). To account for polarizability and charge-transfer effects, the partial charges of the IonL atoms were scaled by 0.8.[43] It is reported that a 0.8 charge scaling factor can accurately capture experimental properties of imidazolium based IonLs such as their bulk density.[43−49]

2.2.2. Ionic Liquid Density. Since the densities of the two IonLs are not available in the literature, they were calculated using MD computer simulations. Following Kuhn et al.,[43] 250 cations and 500 anions were randomly placed in a 50 Å × 50 Å × 50 Å cubic box using Packmol[44] (Figure S2). Periodic boundary conditions were applied in all three directions. First, a 10 ns canonical (NVT) simulation was performed at 300 K to equilibrate the system. Due to the high viscosity and slow dynamics of IonLs, it is necessary to thoroughly mix the molecules and eliminate any energy traps. Hence, annealing simulations were performed by heating the system to 700 K and gradually cooling it to 300 K in 10 K decrements over 10 ns at 1 atm pressure under NPT conditions. Starting from this equilibrated configuration, a 200 ns NPT simulation was performed at 300 K and 1 atm pressure, and the final 60 ns were considered for the density analysis. The density values obtained for IonL-Phe and IonL-Met are given in Table 2.

Table 2. Calculated Ionic Liquid Densities

ionic liquid	density (g/cm^3)
IonL-Phe	1.08
IonL-Met	1.09

2.2.3. Simulation Details. The initial protein configuration was relaxed for 5 ns in water (at an NaCl ionic strength of 0.15 M) following the procedure described in Ranathunga et al.[3] Then, the relaxed protein structure was extracted. The van der Waals volume of the relaxed protein was calculated as 21,253 Å^3 using the Protein Volume web server.[50] The protein was placed on a 84.5 Å × 74.0 Å × 87.0 Å simulation box. Then, the remaining (empty) volume of the box was filled with IonL cations and anions using Packmol,[43,44] neutralizing the total charge of the protein (−5 e charge of HMGB1) and using the calculated IonL densities (see Figure 2c). This model was first relaxed by conjugate gradient energy minimization (5000 steps), followed by an NVT simulation for 2 ns at 300 K. Then annealed by heating the system to 700 K and cooling to 300 K by restraining the protein with a harmonic potential (k = 20 kcal/(mol Å^2)).[51] To further relax the protein and IonL structures, a 5 ns simulation was performed under NPT conditions at 300 K. The relaxed protein/IonL system was combined with the 100% hydroxylated TiO_2 surface. Based on our previous study of HMGB1 in water,[3] the optimal orientation of the protein was chosen with respect to the TiO_2 surface and the initial protein−surface minimum distance was set as 15 Å. Periodic boundary conditions were applied in all three directions. Two repulsive walls were initially maintained

using cylindrical boundary conditions in NAMD at the IonL/vacuum interface and the surface/vacuum interface to prevent molecules from diffusing across the periodic boundary onto the "back" side of the titanium surface. These boundaries were turned off by reducing the force constant gradually to zero within the first 400 ns of the simulation. A 12 Å cutoff was used for the van der Waals and short-ranged electrostatic interactions, while the long-range electrostatics was treated by the Particle Mesh Ewald technique. Energy minimization for 10,000 steps was followed by a 25 ns simulation at 300 K under NVT conditions. Then, to thoroughly mix the IonL molecules and to get rid of any energy traps, the systems were gradually heated (over 10 ns) up to 700 K and cooled (over 90 ns) down to 300 K with the protein and TiO_2 surface atoms constrained to their initial coordinates with springs of force constant k = 20 kcal/ (mol Å^2).[52] These constraints were removed gradually during the last 20 ns of the cooling stage. Subsequently, 2 μs NVT simulations were performed for both IonLs at 300 K. All the simulations were performed using the NAMD software package (v.2.13)[53] and VMD was used for visualization.[54]

2.2.4. Simulations to Study HMGB1 Retention in IonL. To study the protein stabilities in the two selected IonLs, first, the IonL miscibility with water was studied using MD simulations.[55] This was done to verify that the force field gave a realistic representation of the IonLs and IonL/water mixtures. According to the literature, the IonL/ water interface properties may depend on the water model.[56] Several studies report that although the TIP3P water model is widely used to improve computational efficiency, it is known to overestimate the mixing of solvents to some extent.[57] Compared with the TIP3P model, the SPCE-F water model can provide an improved description of the IonL/water mixing properties.[58−60] Therefore, to accurately study the miscibility of the IonLs of interest, the SPCE-F water model was used for the miscibility simulations. To validate the models and methods, an IonL negative control (IonL3) that is known experimentally to be immiscible with water was used. Therefore, the known water immiscible IonL3 ($[C_8MIM_2][NTF_2]_2$) and the IonL-Phe and IonL-Met IonLs were put in contact with water using MD simulations (Figure S5). The parameters used for the $[C_8MIM_2]^{2+}$ cation were obtained from Gross et al.[42] and the NTF_2 anion parameters were taken from Cadena et al.[61] First, 250 cations and 500 anions were randomly placed in a 50 Å × 50 Å × 50 Å cubic box and annealing simulations were performed by heating the system to 700 K and gradually cooling to 300 K temperature in 10 K decrements over 50 ns at 1 atm pressure under isotropic NPT conditions. The equilibrated IonL box was placed next to a similarly sized box filled with 5435 SPCE-F water molecules (Figure S5). Two IonL/water interfaces were generated by using periodic boundary conditions. The simulations were performed in the isotropic NPT ensemble, for 180 ns at 1 atm and 300 K.

To investigate the rate of adsorption/desorption of IonLs from the HMGB1 in water, the previous configuration (Section 2.2.3) of the HMGB1/IonL/TiO_2 system was combined with a 84.45 Å × 74.00 Å × 200.00 Å box filled with SPCE-F water molecules to create the overall unit cell of 84.45 Å × 74.00 Å × 300.00 Å (water volume twice as big as IonL volume). The water box was ionized by adding 0.15 M ionic strength sodium and chloride ions. Periodic boundary conditions were applied in all directions with 10 Å of vacuum both above and below, and two repulsive walls were maintained at the top IonL/vacuum interface and the bottom surface/vacuum interface to prevent molecules from diffusing across the z-periodic boundary. The simulations were performed under NVT conditions, for 300 ns at 300 K.

2.3. Morphological and Physicochemical Characterization. To deduce the HMGB1−IonL interaction sites, liquid chromatography mass spectrometry was employed. Samples were purified using sodium dodecyl sulfate polyacrylamide gel electrophoresis (SDS-PAGE) stained with Coomassie Blue. Liquid-state interactions between IonLs and HMGB1 (25 μg of HMGB1 dissolved in deionized water to a final concentration of 100 μg/μL) with 2.5 mg/ mL IonL in dimethyl sulfoxide-d_6) served as a model for protein binding. Liquid chromatography tandem mass spectrometry (LC−
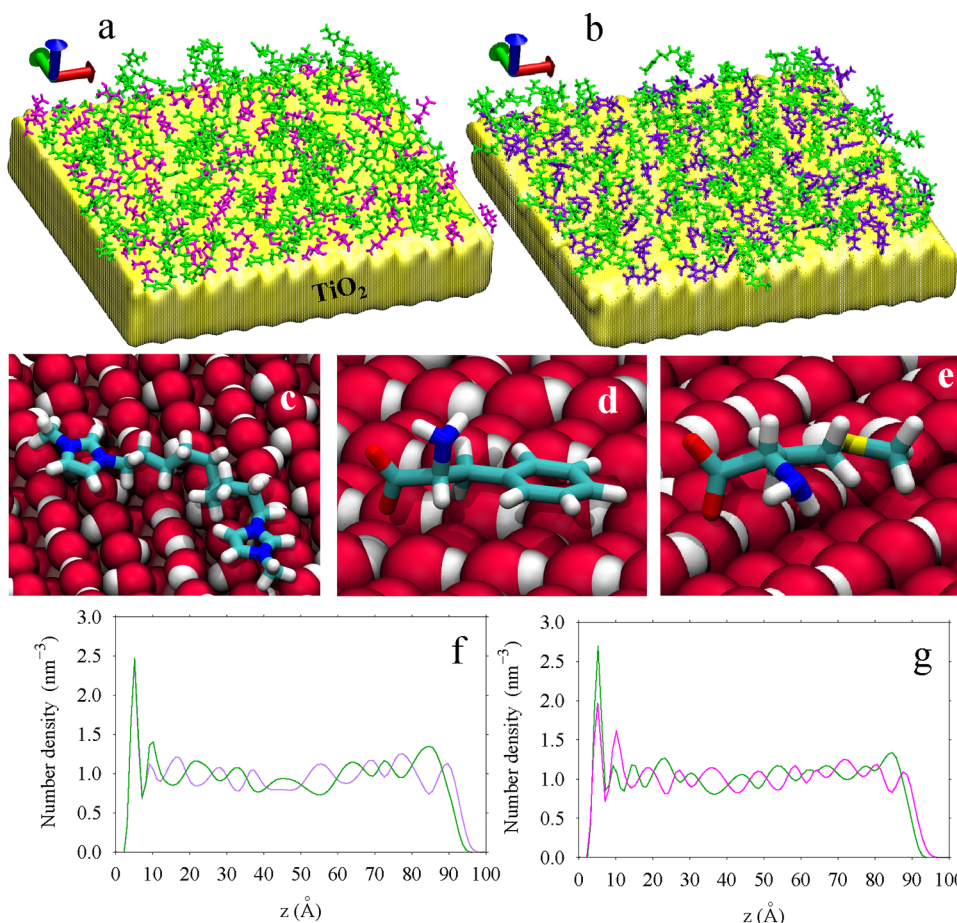
Figure 3. Simulation snapshots of ionic liquids near the TiO$_2$ surface. (a) IonL-Met and (b) IonL-Phe molecules arranged on the surface (di-cation shown in green, phenylalanine shown in purple, methionine shown in magenta, and the TiO$_2$ surface shown in yellow). (c) Imidazole rings are shown oriented parallel to the surface. Most abundant orientations of (d) phenylalanine and (e) methionine anions observed on the surface. Color code is as follows: oxygen atoms in red, titanium atoms in pink, hydrogen atoms in white, carbon atom in cyan, nitrogen atoms in blue, and sulfur atoms in yellow. Number density profile of (f) IonL-Phe and (g) IonL-Met ionic liquids on the TiO$_2$ surface along the z axis. Coloring is as follows: cation (green), phenylalanine (purple), and methionine (magenta).

MS/MS) was used for the structural analysis and identification of binding interactions between the IonL anions and the HMGB1 peptide sequence. Peptide sequences were separated based on their physicochemical properties followed by mass spectroscopy to separate analytes based on a mass-to-charge ratio. Pure HMGB1 suspended in MilliQ deionized water was used as a control and compared to mixtures of HMGB1 with IonL (IonL-Phe or IonL-Met) suspended in MilliQ deionized water. Data was analyzed using Proteome Discoverer 2.4 and was searched using the human protein database from Uniprot for HMGB1. After protease digestion and denaturation, the peptide mass was fingerprinted using the mass-to-charge (m/z) ratio based on molecular weight of the peptide sequences and the charged fragments of the peptide. The sum of the peak intensities for each peptide was identified for HMGB1. These values were then used to compare relative abundance of the pure HMGB1 and were compared to the HMGB1 with ionic liquid mixtures. Additionally, solid-state characterization of surface elemental composition and molecular structuring of HMGB1-IonL coatings and the TiO$_2$ surface were analyzed by X-ray photoelectron spectroscopy (Physical Electronics, Inc., Chanhassen, MN, USA).

IonL density distributions on the TiO$_2$ surface and structural order parameters were measured from the MD simulations. To quantify the protein stability in IonL and specific HMGB1-IonL interactions, H-bond analysis, interaction energy analysis, IonL molecular distribution around the protein, RMSD of the protein in IonL, and contact frequency calculations from the MD data were used. To further quantify the stability of the protein in IonL, the miscibility of IonLs in

water, rate of desorption of IonLs from the protein surface, and the retention capacity of the protein when in contact with water was measured from the MD simulations.

2.3.1. Liquid-State Molecular Characterization. Synthesis of pure IonL-Phe (1,10-bis(3-methylimidazolium-1-yl) decane diphenylala-nine) and IonL-Met (1,10-bis(3-methylimidazolium-1-yl) decane dimethionine) was verified using nuclear magnetic resonance (NMR) (Bruker Avance III-HD 600 NMR, Bruker, Billerica, MA, USA), and results were in accordance with the literature.[28,29] NMR ^{1}H and ^{13}C spectra of pure IonLs diluted in dimethyl sulfoxide-d_6 were recorded (^{1}H at 400.13 MHz and ^{13}C at 100.32 MHz) in 5 mm sample tubes at 298 K (digital resolution of ±0.01 ppm) using TMS as internal reference. Nuclear Magnetic Resonance experiments were performed at 25 °C. For the analysis of each pure IonL compound, 20 mg of IonL was dissolved in 0.7 mL of DMSO-d_6. The NMR peak of DMSO (δ = 2.50 ppm) was used as the reference in determining the chemical shifts of ^{1}H in IonLs.

2.3.2. Liquid Chromatography—Mass Spectrometry. Liquid chromatography mass spectra (LC/MS−MS) of pure IonLs (dissolved in 50 mg/mL of deionized water), pure HMGB1 (dissolved in deionized water at 0.5 mg/mL), and mixtures served as a model for protein binding. Spectra were acquired with Agilent Technologies 6460 Triple quadrupole 6460 (Santa Clara, CA, USA), operated in the positive-ion mode. The gas temperature was 300 °C; the flow of the drying gas was 5 L/min, and the nebulizer was at 45 psi. The voltage of the capillary was 3500 V, and the fragmentor was 0 V. The ionic liquid solutions in H$_2$O were introduced at a 5 μL min^{-1}
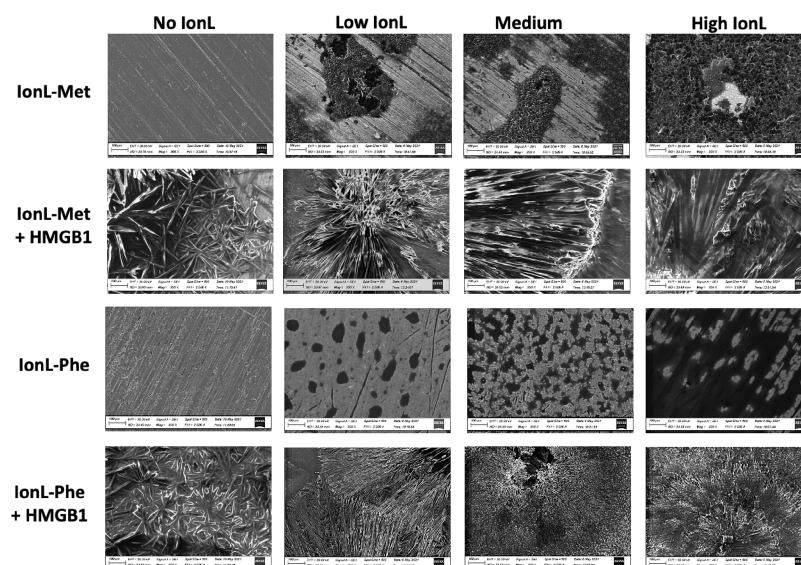
Figure 4. SEM images illustrating ionic liquid coating and HMGB1 behavior on titanium disks at different doses taken at 300× magnification.

flow rate. Nitrogen was used as the nebulization gas, and argon was used as the collision gas.

2.3.3. Solid-State Characterization. Solid-state samples of pure TiO_2, pure IonL-Phe and IonL-Met and the mixture of TiO_2 with HMGB1-IonL (TiO_2 + IonL-Phe-HMGB1 and TiO_2 + IonL-Met-HMGB1) were analyzed by scanning electron microscopy (SEM) (JEOL, JSM6360LV, Akishima, Japan).

2.3.4. Differential Scanning Calorimetry. Differential scanning calorimetry measurements were performed to evaluate the potential for coating stability at physiological temperatures. Solid samples of TiO_2 nanoparticles (<100 nm particle size) coated with IonLs (IonL-Phe and IonL-Met), and mixtures of IonLs and HMGB1 were prepared in equimolar ratios between TiO_2 and IonL and suspended in a total of 5 mL of a 1:1 mixture of ethanol/water w/v. The samples were then stored in the oven at 40 °C for 24 h to remove any residual solvent. Solid samples of pure TiO_2 nanoparticles, pure IonL (IonL-Phe and IonL-Met), the mixture of TiO_2 + IonLs, and the mixture of TiO_2 + IonLs + HMGB1 were analyzed by DSC. The DSC experiments were performed using a MDSC Q2000 (T-zeroTM DSC technology, TA Instruments Inc., New Castle, DE, USA). Dry high-purity (99.999%) nitrogen gas was used as the purge gas (50 mL min^{-1}). The instrument was initially calibrated using the melting point of indium (156.60 °C). The heat capacity calibration was done by running a sapphire standard (α-Al2O3). The heating rate used for all samples was 10 °C min^{-1}. Each IonL was subjected to three cycles of heating and cooling in the temperature range from −80 to 250 °C. Samples were crimped into hermetic aluminum pans with lids and weighed in a precision balance. All glass transition temperatures were detected above 46 °C, indicating that the thermal stability of the compounds would not be altered within an in vivo environment. Glass transition temperatures are shown in Table S1, and the DSC spectra of pure IonL (Met or Phe), Ti nanoparticles coated with IonL, and Ti coated with HMGB1-IonL are shown in Figure S1 and Table S1.

2.3.5. X-ray Photoelectron Spectroscopy. One non-coated control and three HMGB1-IonL-coated TiO_2 specimens (5 mm ø × 2 mm) for each IonL species were analyzed on three different areas per specimen using an X-ray photoelectron spectrometer (XPS, PHI 5000 Versa Probe II, Physical Electronics Inc., Chanhassen, MN, USA). A monochromatic Al K$_\alpha$ source of 1486.6 eV was used, and the measurements were taken at an angle of 45° with respect to the surface of the specimen. The pressure in the analysis chamber was kept below 10−8 torr, and the survey spectra were obtained using a pass energy of 187.850 eV with a 0.8 eV step size. The high-resolution spectra were acquired using a pass energy of 23.5 eV and a step size of 0.2 eV.

2.4. Molecular Dynamics Simulation Analysis. Interaction energy (specifically the electrostatic and van der Waals contributions) between the protein residues and IonL ions were measured using the NAMD energy tool in VMD. Hydrogen bond analysis of IonL ions and protein were calculated using VMD, where a hydrogen bond is considered to exist if the donor−acceptor distance is less than 3.5 Å and the donor−H−acceptor angle is less than 30 degrees. The time averaged density distribution of the IonL ions on the TiO_2 surfaces was measured as a function of the z-distance. The z-distance is defined as the distance from the uppermost titanium atom layer. The average order parameter along the z axis is calculated using eq 1.

$$P_2(\cos\theta) = \left\langle \frac{1}{2}(3\cos^2\theta - 1) \right\rangle \tag{1}$$

where θ is the angle between the normal vector perpendicular to the TiO_2 surface and the vector that passes through the molecule or its aromatic ring, shown in Figures S3 and S4. These angles of cations and anions are defined according to previous literature.[62,63] For contact frequency analysis, salt bridge calculations were performed using VMD and the frequency of finding donor-acceptor atoms within 3.5 Å of each other was measured. More details of the analysis can be found in the Results and Discussion section.

2.5. Statistical Analysis. Statistical significance between non-coated, IonL-coated, and HMGB1-IonL-coated titanium was determined for parameters used to assess coating stability and feasibility. One-way analysis of variance (ANOVA) and post hoc Tukey tests were performed using Origin Pro 8 software (OriginLab Corporation, Northampton, MA, USA), and the between-group means were deemed significantly different for p-values of ≤ 0.05.

3. RESULTS AND DISCUSSION

3.1. Characterization of Surface Coatings. *3.1.1. Molecular Dynamics Characterization of IonL on the TiO_2 Surface.* The molecular structuring of IonL-Phe and IonL-Met cations and anions near the TiO_2 surface was observed in the MD trajectories as shown in Figure 3. Generally, a clear separation of cations and anions into alternating layers near an uncharged solid surface does not occur.[62] If the surface has a net charge, layered IonL structures can form, for example as observed by Sha et al.,[64] where a negatively charged surface tightly adsorbed cations and excluded anions. Nonetheless, for the neutral TiO_2 surface considered here, although both cations and anions occupy the surface, for both IonL-Phe and
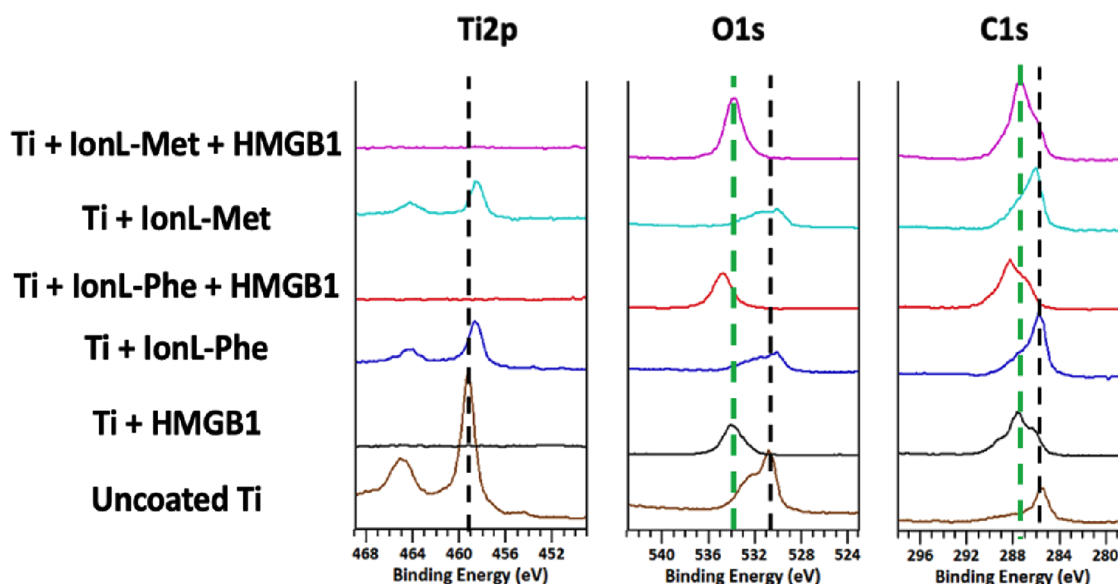
Figure 5. X-ray photoelectron spectra (XPS) of coated and uncoated samples. The overlaid spectra of Ti 2p, O 1s, and C 1s are shown. Elemental peaks corresponding to uncoated Ti control groups are represented by the black dashed line. Elemental peaks corresponding to HMGB1 are represented by the green dashed line.

IonL-Met, a cation-rich behavior at the interface was observed (Figure 3f,g).

To analyze the orientation and structuring of IonL molecules on the surface, the average order parameter along the z axis was measured (see the SI for detailed analysis). Figure 3c−e shows the simulation snapshots of the IonL molecules on the TiO₂ surface and some selected ions to show the most abundant orientations of the imidazolium rings and the anions on the surface. Interestingly, the cations in both IonLs showed similar orientations on the surface. On average, the cationic rings located close to the surface stayed parallel to the TiO₂ surface (Figure S3b and S4b) and most cationic spacer chains also adopted a parallel orientation at the interface (Figure S3c and S4c). It is important to mention that due to the length of the imidazole spacer chain, folding of the molecule is possible.[65] The cation arrangement was mainly due to the electrostatic interactions between the imidazolium ring and the hydroxylated TiO₂ surface.[62] Interestingly in both anions, the COO⁻ group penetrated further into the surface to form hydrogen bonds with the hydroxyls on the surface. Due to the orientation of the COO⁻ group and the benzene ring on the surface, the -NH₂ group of phenylalanine was observed to orient away from the surface (Figure 3d). Figure 3e shows how the methionine anions adsorbed onto the surface of hydroxylated titanium dioxide so that the atoms in both the COO⁻ and NH₂ groups were oriented close to the surface to form hydrogen bonds.

3.1.2. Experimental Morphological Characterization. SEM analysis was used to visualize the coating morphology and characteristics of HMGB1 with respect to different concentrations of IonL on Ti disk samples (Figure 4). At low, medium, and high doses, the pure IonLs exhibited droplet-like formation, potentially exposing Ti to the environment to some extent. At lower doses of pure IonL-Phe and IonL-Met, IonL droplets were observed to be distributed more uniformly along the Ti surface. When higher doses of pure IonL-Phe were used, greater TiO₂ surface coverage was observed due to droplet coalescence. However, pure IonL-Met showed a physical change in property due to

crystallization on the TiO₂ surface with increasing doses. These observations demonstrate that the IonL-Phe was more capable of forming a thin film on the TiO₂ surface as compared to IonL-Met.

When HMGB1 binds to both uncoated and IonL-coated surfaces, a crystal-forming tendency was observed. At low IonL concentration, more crystallization of HMGB1 was also noted. Crystalline formations were less prevalent as the IonL coating increased to medium and high doses (Figure 4). Previous studies have shown that increased alkyl chain lengths of ionic liquids provided the opportunity to crystallize membrane proteins by enforcing surfactant effects, which increased the stability and activity of those proteins.[66,67] Considering the alkyl chain length of the selected IonLs in the current study, protein crystallization on IonL thin films could immobilize and deliver beneficial proteins directly to the sites of implantation.

3.1.3. Solid-State Interactions. The molecular interactions of HMGB1 with IonL on TiO₂ surfaces was evaluated using binding energies measured by XPS and compared to control samples (pure IonLs and control Ti) (Figure 5). It is expected that all surfaces exposed to air will have a thin layer of adventitious carbon material,[68] so all spectra were corrected by internal charge referencing to the aliphatic C 1s photoemission peak (C aliphatic 1s) at 285.0 eV. The oxygen peak was used on the TiO₂ control for comparison with results reported in the literature.[69] The binding energies found for both Ti 2p and O 1s in the TiO₂ control sample were in agreement with the literature.[69] Each pure IonL or IonL with HMGB1 was used to coat three different samples, and three different areas were analyzed per sample. Ti 2p was observed in the uncoated control and in disks coated with pure IonL-Phe or IonL-Met confirming the droplet formation and the exposed Ti areas observed by SEM. The Ti 2p peak was not present in any samples containing HMGB1, indicating a more elevated and fully covered coating profile upon the addition of the protein layer. When Ti 2p was detected in samples coated with IonLs, the binding energies decreased by 0.5 eV.

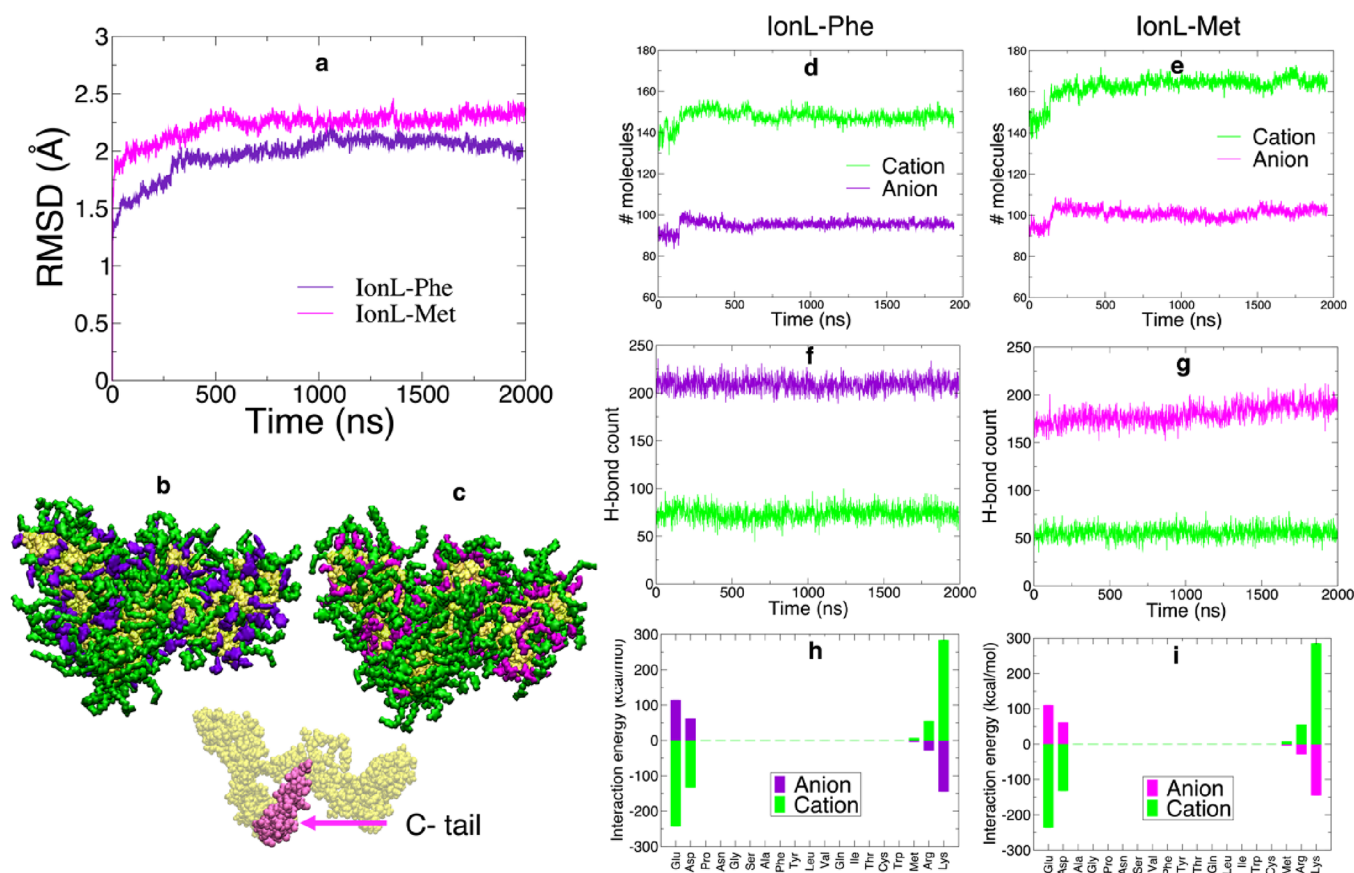The O 1s peak of the uncoated control revealed the TiO₂ layer formation on the implant/disk surface (Figure 5). Also,

Figure 6. (a) Root-mean-square deviation (RMSD) of the protein backbone (C, Cα N) in IonL-Phe and IonL-Met as a function of simulation time. Trajectory snapshots of the distribution of cations and anions within 2.5 Å from the protein surface in (b) IonL-Phe and (c) IonL-Met. Coloring is as follows: all the cations (green), chloride anion (ice blue), phenylalanine anion (purple), methionine anion (magenta), and protein (yellow). Average number of cations and anions in (d) IonL-Phe and (e) IonL-Met systems at less than 5 Å (first solvation shell) from the protein surface at 300 K. Average number of hydrogen bonds between the cations and anions with the protein in (f) IonL-Phe and (g) IonL-Met. Interaction energy strength per IonL anion and cation with the protein amino acids in (h) IonL-Phe and (i) IonL-Met.

Ti 2p was observed in its dioxide state (TiO_2) for the uncoated control Ti. The O 1s peak was consistently seen to have the same binding energy in the IonL-coated samples when compared to the uncoated control. Upon addition of HMGB1 on Ti specimens, the HMGB1 protein layer was observed to completely coat the TiO_2 surface to the extent that Ti 2p was not detected by XPS in samples containing HMGB1. Furthermore, upon the addition of the protein, a distinct O 1s peak was detected approximately 3 eV higher compared to the O 1s peak seen from the TiO_2 layer. There was an increase in binding energies of the C 1s peak observed after HMGB1 deposition onto IonLs in relation to the C 1s peak of the pure IonL thin film. When comparing the Ti + HMGB1 and the Ti + IonL-Phe + HMGB1 spectra, a slight shift of the O 1s and C 1s peaks could be indicative of IonL/HMGB1 interactions with the TiO_2 surface.

The glass transition temperature (Tg) of mixtures can determine the kinetic stability of amorphous solids, which can change due to molecular arrangements and intermolecular interactions.[71] Thermal behaviors of pure IonLs and the mixture of IonLs with HMGB1 were analyzed using DSC (Table S1 and Figure S1). The analysis shows that the glass transition temperatures of the pure IonL-Met (−60.69 °C) and IonL-Phe (−47.71 °C) were not significantly different from IonLs mixed with Ti nanoparticles (IonL-Met +Ti: −61.91 °C, and IonL-Phe + Ti: −46.16 °C), or IonLs mixed with HMGB1

(IonL-Met +HMGB1: −61.21 °C, and IonL-Phe + HMGB1: -47.38 °C). Additionally, Ti nanoparticles were analyzed with a mixture of each IonL + HMGB1, and Tg was not detected. In general, the results did not show significant thermal changes under physiologically relevant conditions.

3.1.4. Molecular Characterization of the IonLs.
3.1.4.1. 1,10-Bis(3-methylimidazolium-1-yl)decane Diphenylalanine (IonL-Phe). $C_{36}H_5 2N_6O_4$, MW: 632.64 g mol^{-1}; ^{1}H NMR (600 MHz, DMSO-d_6): δ 9.70 (s, 2H), 7.81 (s, 2H), 7.74 (s, 2H), 7.20 (m, 8H, phenylalanine), 7.12 (t, 2H, phenylalanine), 4.16 (t, 4H), 3.86 (s, 6H), 3.03 (d, 4H, phenylalanine), 2.43 (t, 2H, phenylalanine), 1.76 (qui, 4H), 1.23 (m, 12H) (Supplementary Figure S7). ^{13}C NMR (125 MHz, DMSO-d_6): δ 142.00 (2C, phenylalanine), 137.90 (2C), 129.68 (2C, phenylalanine), 128.24 (4C, phenylalanine), 125.72 (2C, phenylalanine), 123.99 (2C), 122.68 (2C), 58.53 (2C, phenylalanine), 49.08 (2C), 39.99 (2C, phenylalanine), 36.05 (2C), 29.91 (2C), 29.19 (2C), 28.82 (2C), 25.97 (2C); Tg 47.71 °C (Supplementary Figure S8).

3.1.4.2. 1,10-Bis(3-methylimidazolium-1-yl)decane dimethionine (IonL-Met). $C_{28}H_5 2N_6O_4S_2$, MW: 606.919 g mol^{-1}; ^{1}H NMR (600 MHz, DMSO-d_6): δ 9.73 (s, 2H), 7.83 (s, 2H), 7.75 (s, 2H), 4.18 (t, 4H), 3.88 (s, 6H), 3.21 (d, 2H, methionine), 2.47 (m, 4H, methionine), 2.00 (s, 6H, methionine), 1.78 (t, 6H, methionine), 1.49 (t, 2H), 1.25 (m, 12H) (supplementary Figure S7). ^{13}C NMR (125 MHz,
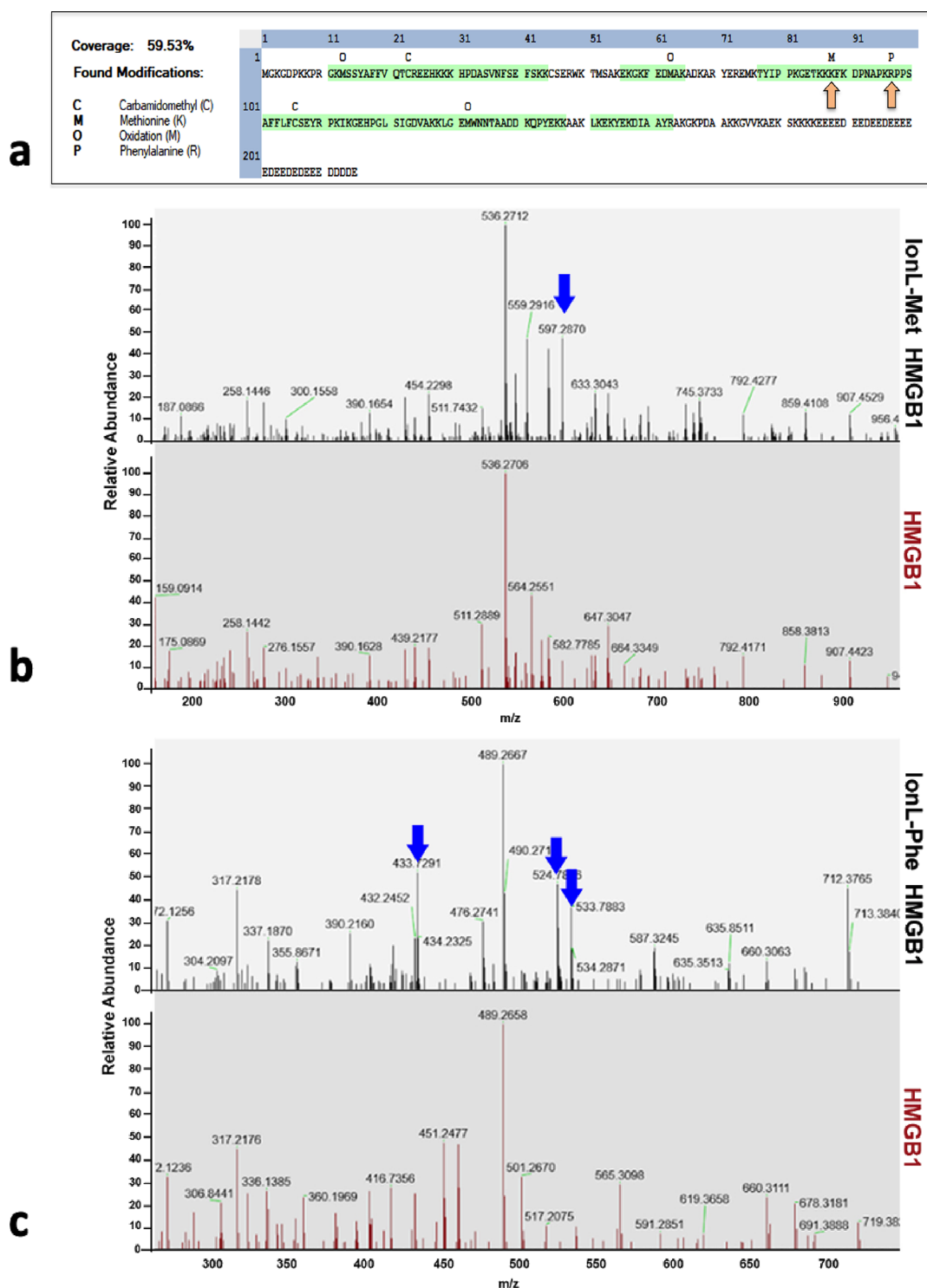
Figure 7. LC−MS/MS separated peptide sequences through a mass to charge ratio. HMGB1 protein card with modifications (a) and spectra of HMGB1-IonL mixtures (black) suspended in DI water were compared to pure HMGB1 (red) suspended in water (b, c).

DMSO-d_6): δ 177.11 (2C, methionine), 137.86 (2C), 124.00 (2C), 122.69 (2C), 56.39 (2C, methionine), 49.11 (2C), 40.00 (2C, methionine), 36.07 (2C), 31.49 (2C, methionine), 29.91 (2C), 29.18 (2C), 28.81 (2C), 25.97 (2C), 15.19 (2C, methionine); Tg 60.69 °C (Supplementary Figure S8).

3.2. HMGB1 Molecular Interactions and Stability. *3.2.1. Computational Analysis of HMGB1 Structural Stability and Interactions.* The strength of the interactions between the HMGB1 protein and the IonL ions can significantly affect the

conformational stability of the protein. First, to examine the structural stability of the protein during the MD simulations, the time-dependent root mean squared deviation (RMSD) of the protein relative to its initial configuration was calculated in both IonL simulations. Figure 6a shows that the protein conformation stabilizes in both IonLs after ∼350 ns into the 2 μs long simulation. Moreover, the percent change in the protein intra-main-chain hydrogen bond count in IonL-Phe and IonL-Met after 2 μs of MD simulation compared to the
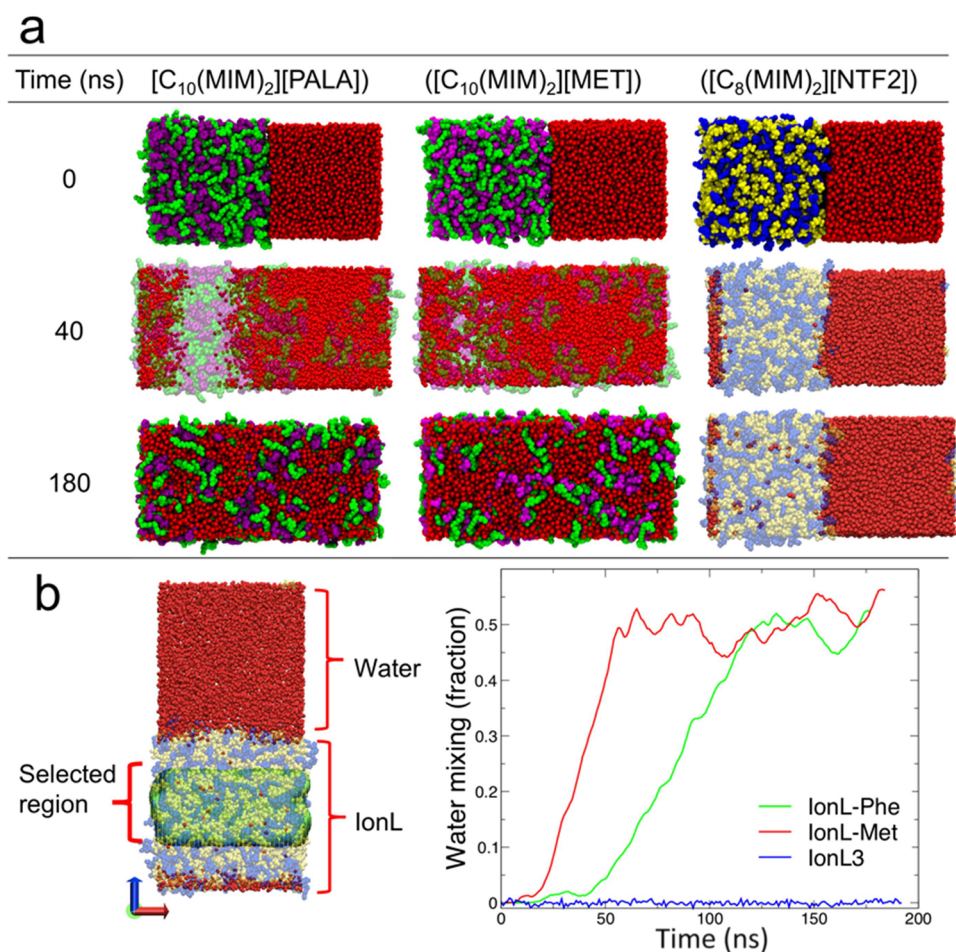
Figure 8. (a) Miscibility results. Van der Waals representation of cations, anions, and water molecules (red) of all three IonL-water mixing simulations. For clarity, hydrogen atoms are not shown. Due to periodic boundary conditions, the IonLs are separated from the water by two interfaces, which are located on the left and right sides of the IonL phase. Some snapshots have a transparent IonL phase to show the mixing clearly. Coloring is as follows: $[C_{10}(MIM)_2]^{2+}$ (green), $[C_8(MIM)_2]^{2+}$ (blue), phenylalanine anion (purple), methionine anion (magenta), and NTF_2 anion (yellow). (b) Water fraction in the selected region for the $[C_{10}MIM_2][PALA]_2$, $[C_{10}MIM_2][MET]_2$, and $[C_8MIM_2][NTF_2]_2$ systems during 180 ns of MD simulation.

initial protein structure in an aqueous environment shown in Table S2 illustrates that the intrachain hydrogen bond network of the protein is only disrupted by 3.7% in IonL-Phe and 9.4% in IonL-Met. These percentage changes in H-bonding after 2 μs demonstrate the higher structural integrity of the protein in IonL-Phe compared to Ion-Met (Table S2).

Furthermore, to understand how the ions around the protein affect its structural integrity, the number of IonL ions in the vicinity of the protein surface (first solvation shell) was studied. More cations were observed on the surface due to the net negative charge of the protein (Figure 6 d and e); in particular, more cations are found around the acidic C-terminal tail (see Figure 6b,c). Figures 6f,g shows that more anions form hydrogen bonds with the protein compared to cations.[72] From MD contact frequency calculations, it was observed that the atoms of the carboxyl groups of Glu and Asp protein residues are more prevalent around the aromatic regions of the IonL cation (Figure S10–S14). The oxygen- and nitrogen-containing moieties in both IonL anions (phenylalanine and methionine) are prevalent near the side chain nitrogen atoms (Figure S10–S14) of the Lys and Arg basic protein residues. The interaction energy calculated by focusing on electrostatic and van der Waals interactions between IonL ions and protein

residues in Figure 6h,i further confirms that the cations strongly interact with the acidic residues of the protein, such as Glu and Asp and the anions strongly interact with the basic residues in the protein, such as Lys and Arg. This indicates that both the cations and anions of IonL distributed around the protein were involved in interactions with oppositely charged amino acid residues.

3.2.2. Characterization of HMGB1 Modifications Using LC−MS/MS. LC−MS/MS findings suggested that HMGB1 binds to both the IonL-Phe and IonL-Met coating in aqueous media. Methionine peptide modifications were observed at the 88th position for the IonL-Met with HMGB1 mixture, while phenylalanine peptide modifications were observed at the 97th position for the IonL-Phe with HMGB1 mixture when each was compared to the pure HMGB1 amino acid sequence. Peptide modifications such as the addition of methionine or the addition of phenylalanine could be indicative of increased affinity or interactions of certain HMGB1 regions to each ionic liquid. Increased affinity or interactions could allow for local delivery of HMGB1 using ionic liquid coatings, harnessing the beneficial roles of this protein directly to the sites of injury. A representative LC−MS/MS protein card with modifications and spectra are shown in Figure 7. The analysis is
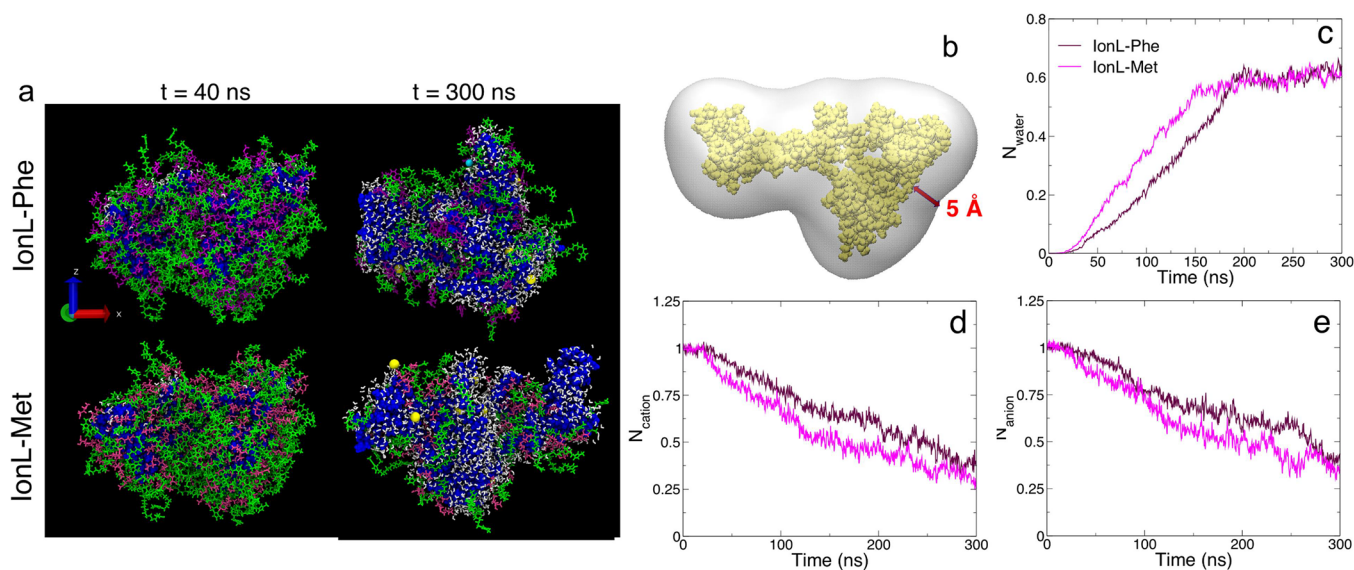
Figure 9. (a) Molecules in the vicinity of HMGB1 versus time. Coloring is as follows: protein (blue), IonL cation (green), phenylalanine anion (purple), methionine anion (magenta), sodium ions (yellow spheres), chloride ions (light-blue spheres), and water (white). (b) Selected 5 Å region (first solvation shell) around the protein. In (c), N_{water} is the fraction of water molecules within 5 Å of the protein surface compared to the HMGB1/water equilibration simulation; in (d), N_{cation} is the fraction of IonL cations within 5 Å of the protein surface compared to the HMGB1/IonL simulation, and in (e), N_{anion} is the fraction of IonL anions within 5 Å of the protein surface compared to the HMGB1/IonL simulation.

representative of approximately 60% of the sequence, seen in green in Figure 7a.

3.2.3. HMGB1 Retention in IonL. To understand which IonL (IonL-Phe or IonL-Met) retained the protein longer on the IonL-coated implant surface, the miscibility of IonL with water was first studied. The accuracy of the chosen water model was verified in the SI using a known water-immiscible IonL, $[C_8MIM_2][NTF2]_2$,[54] which we label as IonL3, as a negative control. In Figure S6, the water density distribution of all three systems at time zero shows a clear water-rich region and a clear IonL-rich region (devoid of water) with a sharp interface between them. During the IonL-Phe and IonL-Met simulations, the two interfacial regions widened until they merged, resulting in clearly observed IonL/water mixing (Figure 8). Supporting these observations, Figure S6 shows how the densities of the two IonL phases change over time. After 180 ns, the final mixture was not homogeneous due to the presence of clusters of ions (Figure 8a and Figure S6).

Figure 8b illustrates the fraction of water in the initially IonL-rich region over time. The progression of X_{water} in Figure 8b suggests that the 180 ns MD simulation was sufficient to equilibrate the IonL-Phe/water and IonL-Met/water systems. In both cases, the mixing with water was completed by the end of the simulation; specifically, the IonL-Phe and IonL-Met systems reached equilibrium after approximately 120 and 75 ns, respectively. This was demonstrated by the plateau value of X_{water} toward a water saturation concentration of roughly 0.5 (Figure 8b). The rate of mixing of IonL-Met was higher than that of IonL-Phe (Figure 8b). Both IonLs contain the same cation and different amino acid-based anions. Therefore, the miscibility difference was due to the effects of the anions. The sulfur atom in methionine was not a hydrogen bond acceptor and showed electronegativity (2.5) similar to that of a carbon atom (2.5). However, the CH_2-S-CH_3 fragment was more polar than the aromatic ring of phenylalanine. According to the hydropathy index of the amino acids that defines the hydrophobic or hydrophilic properties of the side chains, the

more positive hydropathy index of phenylalanine (2.8) represented its greater hydrophobic character compared to methionine (1.9).[70] This supports the observation that the IonL containing methionine showed a higher water solubility compared to the IonL containing phenylalanine.

To further investigate which IonL had the highest protein retention capacity, the rate of adsorption/desorption of IonL on the protein surface was measured. Figure 9a shows how water molecules and NaCl ions replaced the IonL molecules bound to the surface of the protein over time. The protein surface was initially completely covered by IonL molecules, and the water molecules and the Na$^+$ and Cl$^-$ ions subsequently adsorbed on the protein surface over time. After 300 ns, some IonL molecules were still attached to certain amino acid residues on the surface of the protein (Figure 9a). The rate of molecular adsorption/desorption on the protein surface shown in Figure 9 as a function of time illustrates that IonL-Met molecules desorb faster from the protein surface than IonL-Phe molecules. The plateau behavior in Figure 9c was due to the fixed (limited) amount of water in the simulation system. These results suggest that the IonL-Phe coating may retain HMGB1 to a greater extent, or for a longer time, than the IonL-Met coating.

4. CONCLUSIONS

In this study, two different imidazolium-based dicationic ionic liquids, namely, IonL-Met and IonL-Phe, were characterized by means of releasing exogenous HMGB1 protein initially deposited on the surface of a Ti implant. Both IonL-Phe and IonL-Met formed a stable layer on the TiO$_2$ surface. More elevated IonL/HMGB1 coating profiles observed in SEM images and XPS data suggested a fully covered TiO$_2$ surface after coating. Differing concentrations of the coating solution and HMGB1 were found to have an impact on the protein crystallization and coating morphologies. IonL-Phe coatings showed no crystalline formation on the TiO$_2$ surface as opposed to the prevalent crystalline structures seen with

increasing amounts of IonL-Met. Through DSC analysis, coatings were shown to not degrade under temperatures relevant for mammalian applications.

IonL cations and anions interacted with oppositely charged amino acid residues in the protein. These interactions between the HMGB1 protein and the IonL ions significantly affect the protein conformational stability and it retention capability. Both IonL-Phe and IonL-Met coatings were miscible in water. As with any in vitro study, ours has limitations. Although a biological environment was mimicked as closely as possible, it is difficult to completely replicate conditions and complications associated with mechanisms present in living tissue. Fluids present in biological environments could potentially dissolve an implant coating prior to any beneficial outcomes toward healing. Based on the stability of IonL-coated Ti in a previous subcutaneous rat model study,[72] we can predict that the coating will be temporarily present during the acute inflammatory response that lead to healing. Although previous studies have demonstrated both the biocompatibility and stability of IonL-Phe and IonL-Met in Lewis rats,[72] there have not been any previous studies using IonL as an anchoring thin film for HMGB1. To fully understand the impact of IonLs with HMGB1 as coatings (toxicity, biocompatibility, stability, durability, etc.), animal models will be employed in future studies. However, given these limitations, this study does demonstrate that HMGB1 strongly interacted with Ion-Phe and had both higher retention and stability in IonL-Phe compared to IonL-Met. These results point to the potential suitability of IonL as a functional coating and anchoring vehicle for HMGB1 delivery in the context of in vivo immunomodulation.

ASSOCIATED CONTENT

Supporting Information
The Supporting Information is available free of charge at https://pubs.acs.org/doi/10.1021/acs.langmuir.2c02688.

DSC data, hydrogen bond analysis, DSC spectra, IonL density, order parameter results, verification of the accuracy of the chosen water model, IonL solubility setups, IonL/water solubility density, ^{1}H NMR spectra, ^{13}C NMR spectra, quantified data of interacting protein residues, and contact frequency results (PDF)

AUTHOR INFORMATION

Corresponding Author
Danieli C. Rodrigues − Department of Bioengineering, The University of Texas at Dallas, Richardson, Texas 75080, United States; orcid.org/0000-0002-0389-0833; Email: danieli@utdallas.edu

Authors
Alexandra Arteaga − Department of Bioengineering, The University of Texas at Dallas, Richardson, Texas 75080, United States
Dineli T. S. Ranathunga − Department of Chemistry and Biochemistry, The University of Texas at Dallas, Richardson, Texas 75080, United States; orcid.org/0000-0002-7860-722X
Jiayi Qu − School of Dentistry, University of Texas Health San Antonio, San Antonio, Texas 78229, United States
Claudia C. Biguetti − School of Medicine, University of Texas Rio Grande Valley, Edinburg, Texas 78539, United States
Steven O. Nielsen − Department of Chemistry and Biochemistry, The University of Texas at Dallas, Richardson, Texas 75080, United States; orcid.org/0000-0003-3390-3313

Complete contact information is available at:
https://pubs.acs.org/10.1021/acs.langmuir.2c02688

REFERENCES
(1) Saini, M.; Singh, Y.; Arora, P.; Arora, V.; Jain, K. Implant Biomaterials: A Comprehensive Review. World J. Clin. Cases 2015, 3, 52−57.
(2) Brunette, D. M.; Tengvall, P.; Textor, M.; Thomsen, P.Titanium in Medicine : Material Science, Surface Science, Engineering, Biological Responses and Medical Applications; Springer Berlin Heidelberg, 2001.
(3) Ranathunga, D. T. S.; Arteaga, A.; Biguetti, C. C.; Rodrigues, D. C.; Nielsen, S. O. Molecular-Level Understanding of the Influence of Ions and Water on HMGB1 Adsorption Induced by Surface Hydroxylation of Titanium Implants. Langmuir 2021, 37, 10100−10114.
(4) Tsou, H.-K.; Chi, M.-H.; Hung, Y.-W.; Chung, C.-J.; He, J.-L. In Vivo Osseointegration Performance of Titanium Dioxide Coating Modified Polyetheretherketone Using Arc Ion Plating for Spinal Implant Application. Biomed. Res. Int. 2015, 2015, No. 328943.
(5) Stadtman, E. R. Metal Ion-Catalyzed Oxidation of Proteins: Biochemical Mechanism and Biological Consequences. Free Radical Biol. Med. 1990, 9, 315−325.
(6) Anderson, J. M.; Rodriguez, A.; Chang, D. T. Foreign Body Reaction to Biomaterials. Semin. Immunol. 2008, 20, 86−100.
(7) Ziats, N. P.; Miller, K. M.; Anderson, J. M. In Vitro and in Vivo Interactions of Cells with Biomaterials. Biomaterials 1988, 9, 5−13.
(8) Puleo, D. A.; Nanci, A. Understanding and Controlling the Bone−Implant Interface. Biomaterials 1999, 20, 2311−2321.

(9) Jones, L. C.; Tsao, A. K.; Topoleski, L. D. T.Orthopedic Implant Retrieval and Failure Analysis. In *Degradation of Implant Materials*; Eliaz, N., Ed.; Springer Science+Business Media: New York, 2012; pp. 393−447, DOI: 10.1007/978-1-4614-3942-4_15.

(10) Hanawa, T. Titanium−Tissue Interface Reaction and Its Control With Surface Treatment. *Front. Bioeng. Biotechnol.* **2019**, 7, 170.

(11) Okazaki, Y.; Gotoh, E. Metal Release from Stainless Steel, Co−Cr−Mo−Ni−Fe and Ni−Ti Alloys in Vascular Implants. *Corros. Sci.* **2008**, 50, 3429−3438.

(12) Arteaga, A.; Qu, J.; Haynes, S.; Webb, B. G.; LaFontaine, J.; Rodrigues, D. C. Diabetes as a Risk Factor for Orthopedic Implant Surface Performance: A Retrieval and In Vitro Study. *J. Bio Tribocorros* **2021**, 7, 51.

(13) Frankel, G. S. Pitting Corrosion of Metals A Review of the Critical Factors. *J. Electrochem. Soc.* **1998**, 145, 2186−2198.

(14) Wheelis, S. E.; Biguetti, C. C.; Natarajan, S.; Guida, L.; Hedden, B.; Garlet, G. P.; Rodrigues, D. C. Investigation of the Early Healing Response to Dicationic Imidazolium-Based Ionic Liquids: A Biocompatible Coating for Titanium Implants. *ACS Biomater. Sci. Eng.* **2020**, 6, 984−994.

(15) de Mello Gindri, I.Design of Multifunctional Ionic Liquids for Surface Modification of Dental Implants. *ProQuest Dissertations and Theses;*University of Texas2016, 261.

(16) Lu, X.; Wu, Z.; Xu, K.; Wang, X.; Wang, S.; Qiu, H.; Li, X.; Chen, J. Multifunctional Coatings of Titanium Implants Toward Promoting Osseointegration and Preventing Infection: Recent Developments. *Front. Bioeng. Biotechnol.* **2021**, 9, 1093.

(17) Kashiwagi, K.; Tsuji, T.; Shiba, K. Directional BMP-2 for Functionalization of Titanium Surfaces. *Biomaterials* **2009**, 30, 1166−1175.

(18) Wang, J.-J.; Xue, Q.; Wang, Y.-J.; Zhang, M.; Chen, Y.-J.; Zhang, Q. Engineered Chimeric Peptides with IGF-1 and Titanium-Binding Functions to Enhance Osteogenic Differentiation In Vitro under T2DM Condition. *Materials* **2022**, 15, 3134.

(19) Meng, F.; Yin, Z.; Ren, X.; Geng, Z.; Su, J. Construction of Local Drug Delivery System on Titanium-Based Implants to Improve Osseointegration. *Pharmaceutics* **2022**, 14, 1069.

(20) Zhang, B.; Myers, D.; Wallace, G.; Brandt, M.; Choong, P. Bioactive Coatings for Orthopaedic Implants-Recent Trends in Development of Implant Coatings. *Int. J. Mol. Sci.* **2014**, 15, 11878−11921.

(21) Thevenot, P.; Hu, W.; Tang, L. Surface Chemistry Influences Implant Biocompatibility. *Curr. Top. Med. Chem.* **2008**, 8, 270−280.

(22) Anderson, J. L.; Clark, K. D. Ionic Liquids as Tunable Materials in (Bio)Analytical Chemistry. *Anal. Bioanal. Chem.* **2018**, 410, 4565−4566.

(23) Gindri, I. M.; Siddiqui, D. A.; Frizzo, C. P.; Martins, M. A. P.; Rodrigues, D. C. Improvement of Tribological and Anti-Corrosive Performance of Titanium Surfaces Coated with Dicationic Imidazolium-Based Ionic Liquids. *RSC Adv.* **2016**, 6, 78795−78802.

(24) Gindri, I. M.; Frizzo, C. P.; Bender, C. R.; Tier, A. Z.; Martins, M. A. P.; Villetti, M. A.; MacHado, G.; Rodriguez, L. C.; Rodrigues, D. C. Preparation of TiO2 Nanoparticles Coated with Ionic Liquids: A Supramolecular Approach. *ACS Appl. Mater. Interfaces* **2014**, 6, 11536−11543.

(25) Siddiqui, D. A.; Gindri, I. M.; Rodrigues, D. C. Corrosion and Wear Performance of Titanium and Cobalt Chromium Molybdenum Alloys Coated with Dicationic Imidazolium-Based Ionic Liquids. *J. Bio Tribocorros* **2016**, 2, 27.

(26) Gindri, I. M.; Palmer, K. L.; Siddiqui, D. A.; Aghyarian, S.; Frizzo, C. P.; Martins, M. A. P.; Rodrigues, D. C. Evaluation of Mammalian and Bacterial Cell Activity on Titanium Surface Coated with Dicationic Imidazolium-Based Ionic Liquids. *RSC Adv.* **2016**, 6, 36475−36483.

(27) Gindri, I. M.; Siddiqui, D. A.; Frizzo, C. P.; Martins, M. A. P.; Rodrigues, D. C. Ionic Liquid Coatings for Titanium Surfaces: Effect of IL Structure on Coating Profile. *ACS Appl. Mater. Interfaces* **2015**, 7, 27421−27431.

(28) Gindri, I. M.; Siddiqui, D. A.; Bhardwaj, P.; Rodriguez, L. C.; Palmer, K. L.; Frizzo, C. P.; Martins, M. A. P.; Rodrigues, D. C. Dicationic Imidazolium-Based Ionic Liquids: A New Strategy for Non-Toxic and Antimicrobial Materials. *RSC Adv.* **2014**, 4, 62594−62602.

(29) Sandhu, P.; Gindri, I.; Siddiqui, D.; Rodrigues, D. Dicationic Imidazolium-Based Ionic Liquid Coatings on Zirconia Surfaces: Physico-Chemical and Biological Characterization. *J. Funct. Biomater.* **2017**, 8, 50.

(30) Barberi, J.; Spriano, S. Titanium and Protein Adsorption: An Overview of Mechanisms and Effects of Surface Features. *Materials* **2021**, 14, 1590.

(31) Biguetti, C. C.Role of DAMPS on the Modulation of Macrophage Response after Classical Biomaterial (Ti) Implantation and Its Impact on the Subsequent Repair and Osseointegration Process, Faculdade de Odontologia de Bauru; Universidade de São Paulo, São Paulo, 2018. https://pdfs.semanticscholar.org/1617/da70f97a78bd2f584c19ffa5b7a4f1952be0.pdf?_ga=2.245884996.1948194219.1603168727-631109710.1598543658 (accessed 2020-10-18).

(32) Biguetti, C. C.; Cavalla, F.; Silveira, E. V.; Tabanez, A. P.; Francisconi, C. F.; Taga, R.; Campanelli, A. P.; Trombone, A. P. F.; Rodrigues, D. C.; Garlet, G. P. HGMB1 and RAGE as Essential Components of Ti Osseointegration Process in Mice. *Front. Immunol.* **2019**, 10, 709.

(33) Palmquist, A.; Omar, O. M.; Esposito, M.; Lausmaa, J.; Thomsen, P. Titanium Oral Implants: Surface Characteristics, Interface Biology and Clinical Outcome. *J. R. Soc., Interface* **2010**, 7 Suppl 5, S515−S527.

(34) Othman, Z.; Cillero Pastor, B.; van Rijt, S.; Habibovic, P. Understanding Interactions between Biomaterials and Biological Systems Using Proteomics. *Biomaterials* **2018**, 167, 191−204.

(35) Lee, G.; Espirito Santo, A. I.; Zwingenberger, S.; Cai, L.; Vogl, T.; Feldmann, M.; Horwood, N. J.; Chan, J. K.; Nanchahal, J. Fully Reduced HMGB1 Accelerates the Regeneration of Multiple Tissues by Transitioning Stem Cells to GAlert. *Proc. Natl. Acad. Sci. U. S. A.* **2018**, 115, E4463−E4472.

(36) Yang, H.; Antoine, D. J.; Andersson, U.; Tracey, K. J. The Many Faces of HMGB1: Molecular Structure-Functional Activity in Inflammation, Apoptosis, and Chemotaxis. *J. Leukocyte Biol.* **2013**, 93, 865−873.

(37) Schiraldi, M.; Raucci, A.; Muñoz, L. M.; Livoti, E.; Celona, B.; Venereau, E.; Apuzzo, T.; de Marchis, F.; Pedotti, M.; Bachi, A.; Thelen, M.; Varani, L.; Mellado, M.; Proudfoot, A.; Bianchi, M. E.; Uguccioni, M. HMGB1 Promotes Recruitment of Inflammatory Cells to Damaged Tissues by Forming a Complex with CXCL12 and Signaling via CXCR4. *J. Exp. Med.* **2012**, 209, 551−563.

(38) Fukumoto, K.; Yoshizawa, M.; Ohno, H. Room Temperature Ionic Liquids from 20 Natural Amino Acids. *J. Am. Chem. Soc.* **2005**, 127, 2398−2399.

(39) Shirota, H.; Mandai, T.; Fukazawa, H.; Kato, T. Comparison between Dicationic and Monocationic Ionic Liquids: Liquid Density, Thermal Properties, Surface Tension, and Shear Viscosity. *J. Chem. Eng. Data* **2011**, 56, 48.

(40) Karim, M. R.; Li, X.; Kang, P.; Randrianalisoa, J.; Ranathunga, D.; Nielsen, S.; Qin, Z.; Qian, D. Ultrafast Pulsed Laser Induced Nanocrystal Transformation in Colloidal Plasmonic Vesicles. *Adv. Opt. Mater.* **2018**, 6, 1800726.

(41) Brandt, E. G.; Lyubartsev, A. P. Molecular Dynamics Simulations of Adsorption of Amino Acid Side Chain Analogues and a Titanium Binding Peptide on the TiO_2 (100) Surface. *J. Phys.Chem. C* **2015**, 119, 18126−18139.

(42) Gross, A. S.; Bell, A. T.; Chu, J.-W. Thermodynamics of Cellulose Solvation in Water and the Ionic Liquid 1-Butyl-3-Methylimidazolim Chloride. *J. Phys. Chem. B* **2011**, 115, 13433−13440.

(43) Kuhn, B. L.; Osmari, B. F.; Heinen, T. M.; Bonacorso, H. G.; Zanatta, N.; Nielsen, S. O.; Ranathunga, D. T. S.; Villetti, M. A.; Frizzo, C. P. Dicationic Imidazolium-Based Dicarboxylate Ionic

Liquids: Thermophysical Properties and Solubility. *J. Mol. Liq.* **2020**, *308*, No. 112983.

(44) Martínez, L.; Andrade, R.; Birgin, E. G.; Martínez, J. M. PACKMOL: A Package for Building Initial Configurations for Molecular Dynamics Simulations. *J. Comput. Chem.* **2009**, *30*, 2157–2164.

(45) Steudte, S.; Bemowsky, S.; Mahrova, M.; Bottin-Weber, U.; Tojo-Suarez, E.; Stepnowski, P.; Stolte, S. Toxicity and Biodegradability of Dicationic Ionic Liquids. *RSC Adv.* **2014**, *4*, 5198.

(46) Zhou, F.; Liang, Y.; Liu, W. Ionic Liquid Lubricants: Designed Chemistry for Engineering Applications. *Chem. Soc. Rev.* **2009**, *38*, 2590.

(47) Mondal, A.; Balasubramanian, S. A Molecular Dynamics Study of Collective Transport Properties of Imidazolium-Based Room-Temperature Ionic Liquids. *J. Chem. Eng. Data* **2014**, *59*, 3061–3068.

(48) Chaban, V. V.; Voroshylova, I. V.; Kalugin, O. N. A New Force Field Model for the Simulation of Transport Properties of Imidazolium-Based Ionic Liquids. *Phys. Chem. Chem. Phys.* **2011**, *13*, 7910.

(49) Zeindlhofer, V.; Schröder, C. Computational Solvation Analysis of Biomolecules in Aqueous Ionic Liquid Mixtures. *Biophys. Rev.* **2018**, *10*, 825–840.

(50) Chen, C. R.; Makhatadze, G. I. ProteinVolume: Calculating Molecular van Der Waals and Void Volumes in Proteins. *BMC Bioinformatics* **2015**, *16*, 101.

(51) Vanommeslaeghe, K.; Hatcher, E.; Acharya, C.; Kundu, S.; Zhong, S.; Shim, J.; Darian, E.; Guvench, O.; Lopes, P.; Vorobyov, I.; Mackerell, A. D. CHARMM General Force Field: A Force Field for Drug-like Molecules Compatible with the CHARMM All-Atom Additive Biological Force Fields. *J. Comput. Chem.* **2010**, *31*, 671–690.

(52) Phillips, J. C.; Braun, R.; Wang, W.; Gumbart, J.; Tajkhorshid, E.; Villa, E.; Chipot, C.; Skeel, R. D.; Kalé, L.; Schulten, K. Scalable Molecular Dynamics with NAMD. *J. Comput. Chem.* **2005**, *26*, 1781–1802.

(53) Humphrey, W.; Dalke, A.; Schulten, K. VMD: Visual Molecular Dynamics. *J. Mol. Graph.* **1996**, *14*, 33–38.

(54) Klähn, M.; Stüber, C.; Seduraman, A.; Wu, P. What Determines the Miscibility of Ionic Liquids with Water? Identification of the Underlying Factors to Enable a Straightforward Prediction. *J. Phys. Chem. B* **2010**, *114*, 2856–2868.

(55) Bianchi, M. E.; Crippa, M. P.; Manfredi, A. A.; Mezzapelle, R.; Rovere Querini, P.; Venereau, E. High-Mobility Group Box 1 Protein Orchestrates Responses to Tissue Damage via Inflammation, Innate and Adaptive Immunity, and Tissue Repair. *Immunol. Rev.* **2017**, *280*, 74–82.

(56) Sieffert, N.; Wipff, G. The [BMI][Tf2N] Ionic Liquid/Water Binary System: A Molecular Dynamics Study of Phase Separation and of the Liquid−Liquid Interface. *J. Phys. Chem B* **2006**, *110*, 13076.

(57) Chevrot, G.; Schurhammer, R.; Wipff, G. Molecular Dynamics Simulations of the Aqueous Interface with the [BMI][PF6] Ionic Liquid: Comparison of Different Solvent Models. *Phys. Chem. Chem. Phys.* **2006**, *8*, 4166.

(58) Sha, M.; Niu, D.; Dou, Q.; Wu, G.; Fang, H.; Hu, J. Reversible Tuning of the Hydrophobic−Hydrophilic Transition of Hydrophobic Ionic Liquids by Means of an Electric Field. *Soft Matter* **2011**, *7*, 4228.

(59) Serva, A.; Migliorati, V.; Lapi, A.; Aquilanti, G.; Arcovito, A.; D'Angelo, P. Structural Properties of Geminal Dicationic Ionic Liquid/Water Mixtures: A Theoretical and Experimental Insight. *Phys. Chem. Chem. Phys.* **2016**, *18*, 16544–16554.

(60) Cadena, C.; Zhao, Q.; Snurr, R. Q.; Maginn, E. J.Molecular Modeling and Experimental Studies of the Thermodynamic and Transport Properties of Pyridinium-Based Ionic Liquids. 2006, 2821, DOI: 10.1021/JP056235K.

(61) Malali, S.; Foroutan, M. Study of Wetting Behavior of $BMIM^+$/PF_6^- Ionic Liquid on TiO_2 (110) Surface by Molecular Dynamics Simulation. *J. Phys. Chem. C* **2017**, *121*, 11226–11233.

(62) Li, S.; Feng, G.; Cummings, P. T. Interfaces of Dicationic Ionic Liquids and Graphene: A Molecular Dynamics Simulation Study. *J. Phys.: Condens. Matter* **2014**, *26*, No. 284106.

(63) Sha, M.; Wu, G.; Dou, Q.; Tang, Z.; Fang, H. Double-Layer Formation of [Bmim][PF6] Ionic Liquid Triggered by Surface Negative Charge. *Langmuir* **2010**, *26*, 12667−12672.

(64) Frizzo, C. P.; Bender, C. R.; Gindri, I. D. M.; Villetti, M. A.; Machado, G.; Bianchi, O.; Martins, M. A. P. Elucidating Anion Effect on Nanostructural Organization of Dicationic Imidazolium-Based Ionic Liquids. *J. Phys. Chem. C* **2016**, *120*, 14402−14409.

(65) Alizadeh, A.; Bahadur, V.; Kulkarni, A.; Yamada, M.; Ruud, J. A. Hydrophobic Surfaces for Control and Enhancement of Water Phase Transitions. *MRS Bull* **2013**, *38*, 407−411.

(66) Allen, M. P.; Tildesley, D. J.*Computer Simulation of Liquids*; Clarendon Press, 1987.

(67) Belviso, B. D.; Caliandro, R.; Salehi, S. M.; Di Profio, G.; Caliandro, R. Protein Crystallization in Ionic-Liquid Hydrogel Composite Membranes. *Crystals* **2019**, *9*, 253.

(68) Schröder, C. Proteins in Ionic Liquids: Current Status of Experiments and Simulations. *Top. Curr. Chem.* **2017**, *375*, 25.

(69) Greczynski, G.; Hultman, L. C 1s Peak of Adventitious Carbon Aligns to the Vacuum Level: Dire Consequences for Material's Bonding Assignment by Photoelectron Spectroscopy. *ChemPhysChem* **2017**, *18*, 1507−1512.

(70) Biesinger, M. C.; Lau, L. W.; Gerson, A. R.; StC Smart, R. Resolving Surface Chemical States in XPS Analysis of First Row Transition Metals, Oxides and Hydroxides: Sc, Ti, V, Cu and Zn. *Appl. Surf. Sci.* **2010**, *257*, 887−898.

(71) Kyte, J.; Doolittle, R. F. A Simple Method for Displaying the Hydropathic Character of a Protein. *J. Mol. Biol.* **1982**, *157*, 105−132.

(72) Wheelis, S. E.; Biguetti, C. C.; Natarajan, S.; Lakkasetter Chandrashekar, B.; Arteaga, A.; El Allami, J.; Garlet, G. P.; Rodrigues, D. C. Effects of Dicationic Imidazolium-Based Ionic Liquids on Oral Osseointegration of Titanium Implants: An in Vivo Biocompatibility Study in Multiple Rat Demographics. *Genes* **2022**, *13*, 642.

📖 Recommended by ACS